JOURNAL OF MAGNETIC RESONANCE **130,** 102–110 (1998)
ARTICLE NO. MN971264

An Alternative Scheme for ^{13}C Chemical-Shift Imaging via Inverse Detection of Protons through an MILS (or Inverse SLIM) Technique

Shu-Ming Lee, Der-Lii Tzou,[1] George J. Y. Chiou, and Hong N. Yeung†

Institute of Biomedical Sciences, Academia Sinica, Taipei, 11529 Taiwan, Republic of China

Received May 20, 1997; revised August 20, 1997

An alternative scheme in acquiring ^{13}C spectroscopic images using inverse detection via polarization transfer through protons was proposed and experimentally verified by a phantom using a heteronuclear multiple-quantum coherence technique. This scheme has some features that, in special circumstances, can be exploited to one's advantages. These features are: (1) signal enhancement, a feat realizable under favorable conditions; (2) spectroscopic encoding via constant time; and (3) improvement of the time efficiency of the constant-time method via optimization by singular-value decomposition analysis. Features (1) and (2) can, in some cases, yield better sensitivity than the conventional 3DFT technique without sacrificing the most important attribute of ^{13}C, the enormity of the chemical shifts. Such is the case because spectroscopic images acquired by the technique proposed are based on the chemical shifts of carbon, in contrast to the other more prevalent inverse-detection schemes. Feature (2) can also offer higher spatial resolution by shifting the emphasis of signal encoding from a spectral-resolution-first viewpoint to one that favors spatial resolution. Feature (3) was adopted from a method previously known as MILS (metabolite imaging of lines in a spectrum), or the inverse of SLIM, an economical scheme originally proposed by Hu *et al.* (1988, *Magn. Reson. Med.* 8, 314) for obtaining a compartmentalized NMR spectrum.

INTRODUCTION

In vivo ^{13}C magnetic resonance spectroscopy has been found to be increasingly important in biological applications as exemplified by its role in the elucidation of the metabolism of carbohydrates and fatty acids in liver and brain (*1*). To obtain spatial as well as spectral distribution for these carbon moieties, imaging development in ^{13}C, since its early attempt (*2*) using a standard technique a decade ago, has also been progressing (*3–11*). In these more recent developments, the feasibility of *in vivo* spectroscopic imaging in humans has been demonstrated in natural abundance by conventional means using coplanar concentric surface coils (*7*). In other studies, proton-enhanced schemes by polarization transfer were often used to boost signal sensitivity (*9–11*). The main difficulty of ^{13}C imaging and spectroscopy, particularly under *in vivo* conditions, is the low sensitivity caused by the low gyromagnetic ratio and low natural abundance of the nuclide. However, these drawbacks are not entirely detrimental. For example, being low in natural abundance can sometimes be turned into an advantage since it allows the option of monitoring events occurring in specific metabolic pathways via the administration of a precursor, e.g., glucose, with a ^{13}C label strategically placed in a particular position. The increasing availability of high-field imaging spectrometers and the use of proton-enhanced schemes also alleviate significantly the problem of poor sensitivity. Nevertheless, despite some of these positive exploitable attributes and technical improvements, the problem remains formidable for *in vivo* applications because of the constraint in scan time.

In this article, an alternative method of acquiring chemical-shift images of ^{13}C based on inversion detection via heteronuclear multiple-quantum coherence (HMQC) (*12*) is proposed. The HMQC sequence, common to all polarization transfer techniques, offers the advantage of signal enhancement, realizable if certain experimental conditions, such as having long T_2 in the moieties of interest, are met. Furthermore, spectral and spatial encoding in this scheme is implemented in a way similar to the generalized Dixon fat–water separation scheme (*13*) first proposed by Sepponen *et al.* (*14*) and Cho *et al.* (*15*), which is, in essence, an imaging version of the constant-time technique proposed even earlier by Bax *et al.* (*16*). Finally, to reduce scan time, a scheme analogous to the SLIM technique employed by Hu *et al.* (*17*) for compartmentalized spectroscopy is adopted. Our scheme, first applied to proton CSI (*18*), is actually an inverse of SLIM, or MILS, which stands for metabolic imaging of lines in a spectrum. In essence, the method entails the acquisition of a set of images, taken at different evolution periods, t_1, strategically and parsimoniously chosen for their effectiveness in resolving spectral differences for a given spectrum by the constant-time scheme. The criterion used to determine the optimal set of incremental time displace-

[1] To whom correspondence should be addressed. Fax: 886-2-2788-7641.

† Dr. Hong N. Yeung died from illness on October 6, 1997. Dr. Lee, Dr. Tzou, and Dr. Chiou dedicate this work to the memory of Dr. Yeung for his endless passion for doing scientific research and for his more than twenty years of contributions in the field of MRI.

1090-7807/98 $25.00

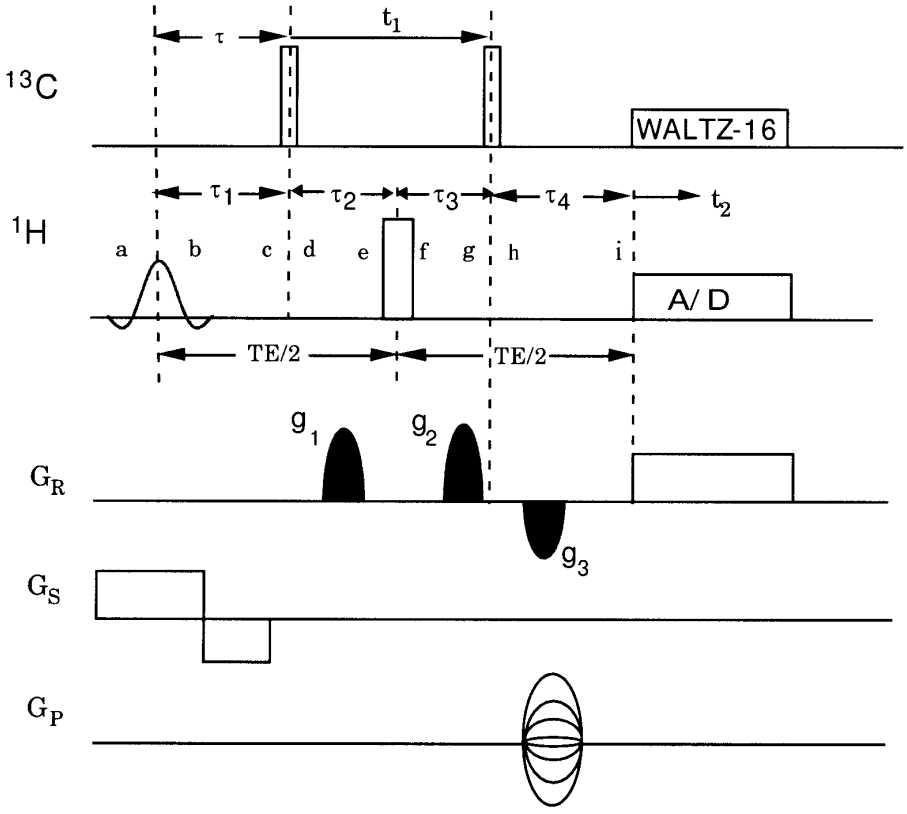

FIG. 1. Pulse sequence for spectroscopic imaging of insensitive nuclides using heteronuclear multiple-quantum coherence in a constant-time technique. The increment of timing variable t_1 is used as a means of encoding the ^{13}C spectral information. See text for detailed discussions on the optimization scheme for the time increments as well as the other timing parameters.

ments δt_1 is based on a statistical procedure known as singular-value decomposition (*19*).

Our goal here is to demonstrate experimentally, using a simple phantom, the feasibility and potential benefit of this alternative scheme when it is extended to the acquisition of ^{13}C images of spectral lines via inverse detection using heteronuclear multiple-quantum coherence (*4–6, 8–12*).

METHOD AND MATERIALS

The HMQC imaging sequence used in our experiment and shown in Fig. 1 is essentially the same as those employed in many previous works (*4–6, 8–11*). The only feature pertinent to the ^{13}C-based CSI scheme worth pointing out is the time period t_1, separating the two carbon 90° pulses. It is this period, in our scheme, which is incremented on sequence repetition, and it is these time increments that give the ^{13}C imaging data the spectral encoding. During this period, the 180° pulse applied on a proton is mainly to generate a spin echo and thereby eliminate any effects caused by proton chemical shifts and main-field inhomogeneities. Note that the application of such a proton refocusing pulse during this period has the effect of switching the zero-quantum coherence to double-quantum coherence and vice versa, but it has no effect at all on the evolution experienced by the ^{13}C chemical-shift Hamiltonian. To contrast this ^{13}C-based CSI scheme to the more prevalent ^{1}H-based method (*11*), experimental runs were also conducted on the same phantom but using a version of the sequence in which t_1 is held constant while the timing of the 180° proton pulse is varied. The chemical-shift images obtained by this procedure, though still commonly referred to in the literature as ''carbon CSI,'' are in effect images based on the chemical shifts of protons that are coupled to the carbon moieties.

The algebraic expression associated with the HMQC sequence is of course well known (*12*) and expositions on the different aspects of its adaptation for imaging applications have, to different degrees of thoroughness, also been given (*6, 8*). By way of background, the part of the spin coherence that is pertinent to our present development, from its initial state characterized by the spin density matrix $\sigma(0)$ to its evolution to the point of observation $\sigma(\mathrm{TE})$, where TE is the time of the echo formation, is succinctly outlined here. This time development, $\sigma(0) \rightarrow \sigma(\mathrm{TE})$, as prescribed according to the pulse sequence of Fig. 1, can be evaluated by the usual product operator formalism, bearing in mind that,

in the free precession periods, the governing Hamiltonian of the spin system, in the presence of magnetic field gradient, is given by

$$H = \delta_I I_z + \delta_S S_z + J_{CH} I_z S_z + (\gamma_I I_z + \gamma_S S_z)\mathbf{x}\cdot\mathbf{G}_\Theta;$$
$$\delta_\alpha = -\gamma_\alpha(1 - \sigma_\alpha)H_0, \qquad [1]$$

where $\alpha = I, S$, in which I stands for ^{1}H and S, ^{13}C; $\mathbf{x}$ is the position vector; and $\mathbf{G}_\Theta$ is the field-gradient vector employed to select the order of the multiple-quantum coherence with which images were formed. The parts of the spin density matrix that yield proton signals can be shown to be given by a sum of three terms classified according to their respective orders of MQC before their back-conversion to single-quantum coherence by the second 90° pulse applied to the carbon spins,

$$\sigma(\mathrm{TE}) = \Sigma^{(0)} + \Sigma^{(1)} + \Sigma^{(2)}, \qquad [2]$$

where the superscripts of Σ indicate the order of MQC. Detailed expressions of their amplitude and phase factors can be written as

$$\Sigma^{(0)} = \sin\theta_1\cos\theta_2\cos\theta_3\cos(\theta_2 - \theta_3) \times \sin\theta_4(e^{-i\phi^{(0)}}I_- + \text{c.c.})$$
$$\Sigma^{(1)} = \cos\theta_1\cos\theta_2\cos\theta_3\cos\theta_4(e^{-i\phi^{(1)}}I_- - \text{c.c.})$$
$$\Sigma^{(2)} = \sin\theta_1\cos\theta_2\cos\theta_3\cos(\theta_2 - \theta_3) \times \sin\theta_4(e^{i\phi^{(2)}}I_+ + \text{c.c.}) \qquad [3]$$

with

$$\theta_j = \pi J_{CH}\tau_j; \qquad [4]$$

$$\tau_1 = \tau = \frac{1}{2J_{CH}}, \quad \tau_2 = \frac{\mathrm{TE}}{2} - \tau,$$

$$\tau_3 = t_1 - \tau_2, \quad \tau_4 = \frac{\mathrm{TE}}{2} - \tau_3 \qquad [5]$$

$$\phi^{(0)} = -\delta_s t_1 + \mathbf{x}\cdot\mathbf{k}^{(0)}$$
$$\phi^{(1)} = \mathbf{x}\cdot\mathbf{k}^{(1)} \qquad [6]$$
$$\phi^{(2)} = \delta_s t_1 + \mathbf{x}\cdot\mathbf{k}^{(2)}$$

$$\mathbf{k}^{(j)} = -a^{(j)}\int \mathbf{g}_1(s)ds + b^{(j)}\int \mathbf{g}_2(s)ds - \mathbf{k}_{RG} \qquad [7]$$

$$a^{(0)} = b^{(2)} = \gamma_I + \gamma_S, \quad b^{(0)} = a^{(2)} = \gamma_I - \gamma_S \qquad [8]$$

$$a^{(1)} = b^{(1)} = \gamma_I \qquad [9]$$

$$\mathbf{k}_{RG} = \gamma_I\left(\int \mathbf{g}_3(s)ds - \mathbf{G}_R\frac{T_{acq}}{2}\right), \qquad [10]$$

where the integral in [7] and [10] means the area under the curve of the shaped gradients, and the last term in [7], defined in [10], represents the net phase angle that the proton isochromats traverse during the rephasing and dephasing part of the read-gradient events that occurred just before the echo formation. To select the zero- or double-quantum coherence to form images, the strategy is then simply to choose a particular combination of $\mathbf{g}_1$, $\mathbf{g}_2$, and $\mathbf{g}_3$ such that $\mathbf{k}^{(0)}$ or $\mathbf{k}^{(2)} = 0$ while leaving $|\mathbf{k}^{(m)}|$, $m \neq 0$ or 2, so large that the signal of the mth-quantum coherence will not occur within the sampling window.

There are two more points worth noting concerning Eq. [3]: The first is that both phase angles $\phi^{(0)}$ and $\phi^{(2)}$ contain a term formed by the product of the carbon chemical shift and the evolution time t_1, reaffirming what has been said earlier. By virtue of this relation, chemical-shift images based on carbon, rather than a proton, can be generated by incrementing t_1 as a result. It is precisely this attribute that makes the ^{13}C MILS technique advantageous over its competitors, FT CSI in conventional implementation or in SLIM using inverse detection of the proton. The second is that the criterion for the optimal choice of the timing parameters τ_j, $j = 1, 2, 3, 4$, for the zero- and double-quantum coherence is that the angles θ_j, defined in Eq. [4], are odd multiples of $\pi/2$ for θ_1 and θ_4, and multiples of π for θ_2 and θ_3. In other words, the optimal timing for MQC is

$$\tau_1 = \tau_4 = (2n - 1)(2J_{CH})^{-1}, \qquad [11a]$$
$$\tau_2 = \tau_3 = nJ_{CH}^{-1}, \quad \text{with } n \text{ being any integer larger than or equal to 1.} \qquad [11b]$$

There are two sides to the effects of these relationships. The positive side is that they provide a means of editing the intensities of the chemical-shift component images to be formed according to the coupling constants. The negative side is that if the opposite is desired, i.e., if intensity is required to reflect only moiety concentration, then it is often difficult to find a set of timing parameters, as we shall show under Results below, to fulfill such a requirement unless the J_{CH} constants of these moieties happen to fall within a narrow range.

All NMR experiments were performed on a Bruker 400-MHz AMX wide-bore (8.9-cm) system (Bruker Spectrospin, Fällanden, Switzerland) with micro-imaging probe accessories. The most essential part of the probe assembly is a ^{1}H–^{13}C double-tuned coil which consists of two pairs of saddle-shaped loops, with the inner pair tuned to the carbon, and the outer pair, to the proton frequency. The two pairs, with loops diametrically opposed, are skewed relatively 90° apart from one another to minimize inductive coupling. The bore diameter allowed by the inner loop is approximately 12 mm. The phantom used consists of four small sample tubes (three

with an o.d. of 2 mm, and one with an o.d. of 5 mm), each filled with different carbon containing chemicals: C1-enriched glucose (99%, Cambridge Isotope Lab., Andover, MA), natural-abundant ethylene glycol, enriched sodium formate (99%, CIL), and natural-abundant 2-propanol. Both the glucose and the sodium formate were dissolved in D_2O. They were inserted into a 10-mm-i.d. NMR tube filled with water. Before acquiring ^{13}C imaging data using the MILS sequence, a conventional spin-echo proton image and a proton-decoupled ^{13}C spectrum of the phantom were obtained. The former serves to illustrate the geometrical arrangement of the phantom components and the latter, the required input for the determination of the optimized timings $\{t_1\}$ for the MILS. The timing parameters used in the pulse sequence, as shown in Fig. 1, are $\tau = \tau_1 = \tau_4 = 2.994$ ms, $\tau_2 = \tau_3 = 5.988$ ms, and TE $= 2(\tau_1 + \tau_2) = 17.964$ ms. The recycle delay, TR, used in this set of experiments is 3 s. No slice selection was used in these experimental runs (i.e., the slice selection gradient was set to 0). The field-of-view (FOV) of the images is 1.2 cm with a matrix size of 64×32, with the second being the number of phase-encoding steps. By running each pulse sequence repeatedly four times for signal accumulation and phase cycling, the scan time of image formation for each t_1 is therefore $4 \times 32 \times 3$ s $= 384$ s or 6.4 min.

From our previous work (*18*) on proton CSI by this scheme, it had been found that the choice of the time displacements $\{\delta t_{1j}\}$, $j = 1, 2, \ldots N$, for a given set of M lines in a spectrum, where $N \geq M$, could be optimized, according to the line separations in the input spectrum. This optimization is based on the criterion that the condition number κ, defined as the largest singular value divided by the smallest, must be the smallest or, since by definition, $\kappa \geq 1$, closest to 1. In addition to this optimization program, one also needs an image-unraveling program to untangle the t_1-encoded input images into the desirable output—a set of images corresponding to the spectrally separable components. A full description of this optimization and unraveling scheme and a detailed listing of all the necessary computer programs designed for the MILS applications were given by Li (*20*), and were implemented in our laboratory with slight modifications in a Matlab environment (Mathworks, Inc., Natick, MA). For the case of protons, because of the minuteness of the chemical shifts, one often needs to be overdetermined, i.e., having N larger than M, to yield satisfactory results. For ^{13}C, however, because of its much larger chemical shifts, the more parsimonious condition, $N = M$, was found to be adequate to give good separation on all component images corresponding to the well-resolved lines in the spectrum, as can be demonstrated by the results to be shown below.

RESULTS

Before discussing the experimental results, the atomic concentration of ^{13}C in the phantom needs to be clarified. At issue is the use of the 99% enriched compounds and the naturally abundant neat liquids since this means that the sample ^{13}C concentrations are a thousand-fold of what one would probably find in tissues, even with enrichment. At first glance, this seems to be quite unrealistic, until one figures, from the imaging parameters given above, that the voxels in images given below all have a volume under 1 μl which is approximately a thousandth of the voxel size typically used in *in vivo* studies.

The proton image of the phantom used in our study is shown in Fig. 2 and the corresponding proton-decoupled ^{13}C spectrum is shown in Fig. 3. According to the ^{13}C chemical shifts shown in this figure, there are four groups of well-resolved spectral lines which correspond, almost one-to-one, to a set of spatially separated moieties as identified and labeled separately in Figs. 2 and 3 (see description given in the figure legend for the detailed assignments). Since there are four groups of well-resolved spectral lines in Fig. 3 (note that the spectral dual corresponding to the α- and β-forms of C1-glucose are lumped together as a single entity here), the most economical data collection scheme in this case calls for four input images (shown in Fig. 4a) with a corresponding set of optimized time displacements found to be -116.16, -59.48, 55.27, and 111.96 μs, the condition number being $\kappa = 1.9$. With this time-displacement set, the outcome of the cleanly separated chemical-shift images are shown in Fig. 4b. Before commenting on the issue of the separability of spectral components by this procedure, it should be noted that not a trace of the water intensity is observed in the input images, demonstrating the powerful effect of solvent suppression of multiple-quantum filtering.

To appraise this result in proper perspective, one needs to compare it with two types of experimental runs for the same objective. The first type is simply the unoptimized runs of the same experiment by picking different sets of $\{\delta t_1\}$ that have higher κ. As pointed out in our earlier work (*18*), the effect caused by a nonideal timing set, as reflected by an increase in the condition number κ, is that any experimental imperfections such as noise and spatial/spectral misregistration (given rise by the main-field susceptibilities, inhomogeneities, and/or gradient errors) will become amplified in the unraveling process. This amplification of aberrations has two undesirable consequences: (i) image ''contamination'' which generates ghost images occurring in sample compartments where they do not belong, and (ii) an increase in image noise. In the case of proton CSI (or for that matter, ^{1}H-based ^{13}C CSI, see below), the first side effect, i.e., image contamination, is more notably observed. In the case of ^{13}C CSI using a genuinely ^{13}C-based technique, however, the quality of image separation is not at all sensitive to the choice of the encoding times in contrast to the ^{1}H-based method. The deterioration of image quality under nonideal conditions arises mainly then from the noise amplification. These observations are the results, succinctly summarized

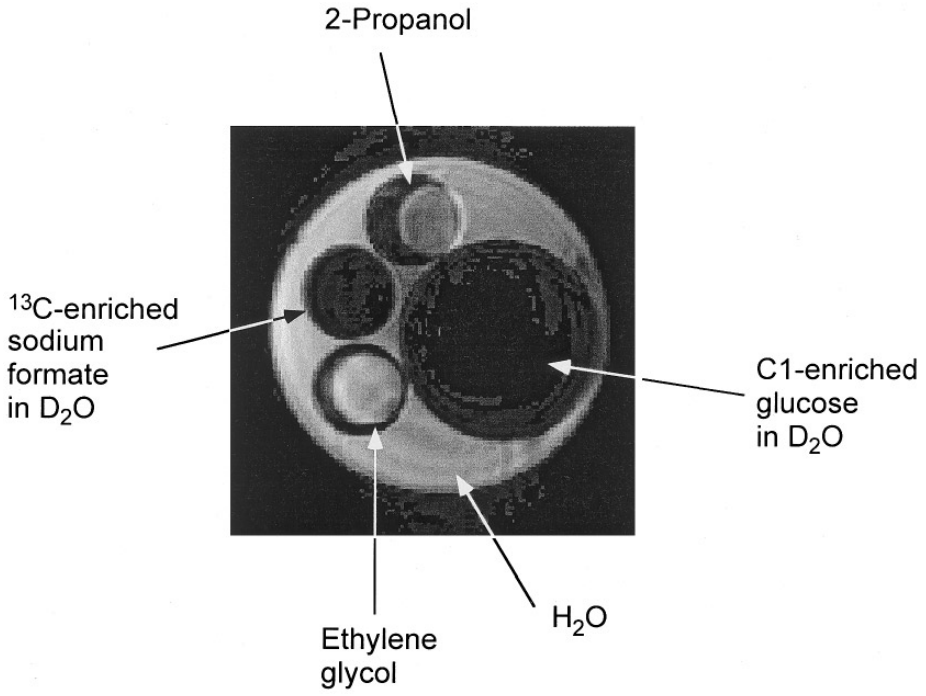

FIG. 2. Proton image of the phantom used in the study. The compounds contained in the sample tubes are identified as shown. Note incidentally the prominent chemical-shift artifacts in the frequency-encoding direction of the image. The effect of heteronuclear *J* coupling is suppressed by the relatively large pixel bandwidth of the image.

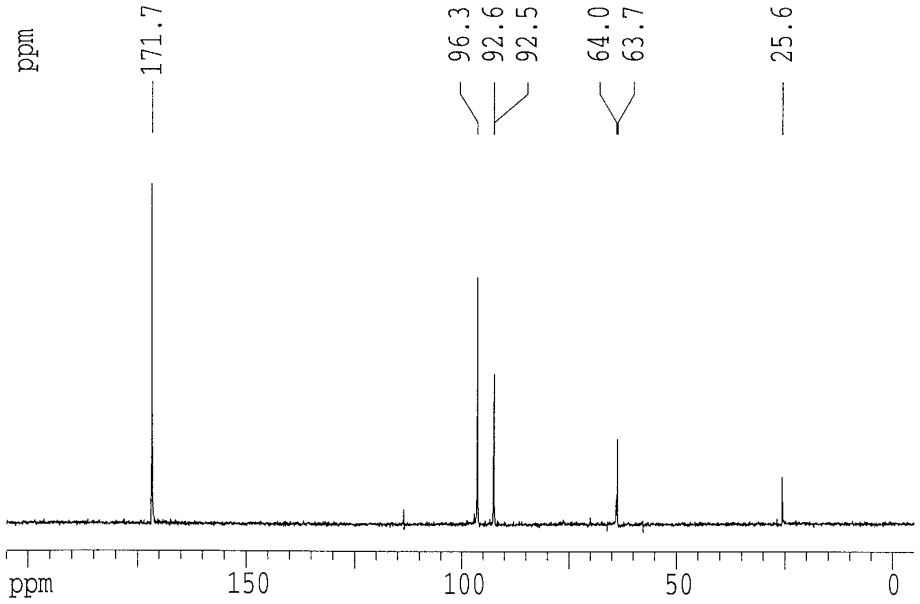

FIG. 3. Proton-decoupled ^{13}C spectrum of the phantom. The spectral lines of ethylene glycol (at 63.7 ppm) and the enriched sodium formate (171.7 ppm) are singlets; the two closely spaced lines (3.8 ppm apart) at around 95 ppm are the α- and β-forms of the enriched C1-glucose. The two lines associated with 2-propanol corresponding to the methyl and C2-carbon (with an intensity ratio somewhat less than the theoretical value 6:1) have chemical-shift values of 25.6 and 64.0 ppm; the latter falls fortuitously and almost exactly on the same position as that of ethylene glycol. (All ppm values are referenced with respect to tetramethylsilane.)

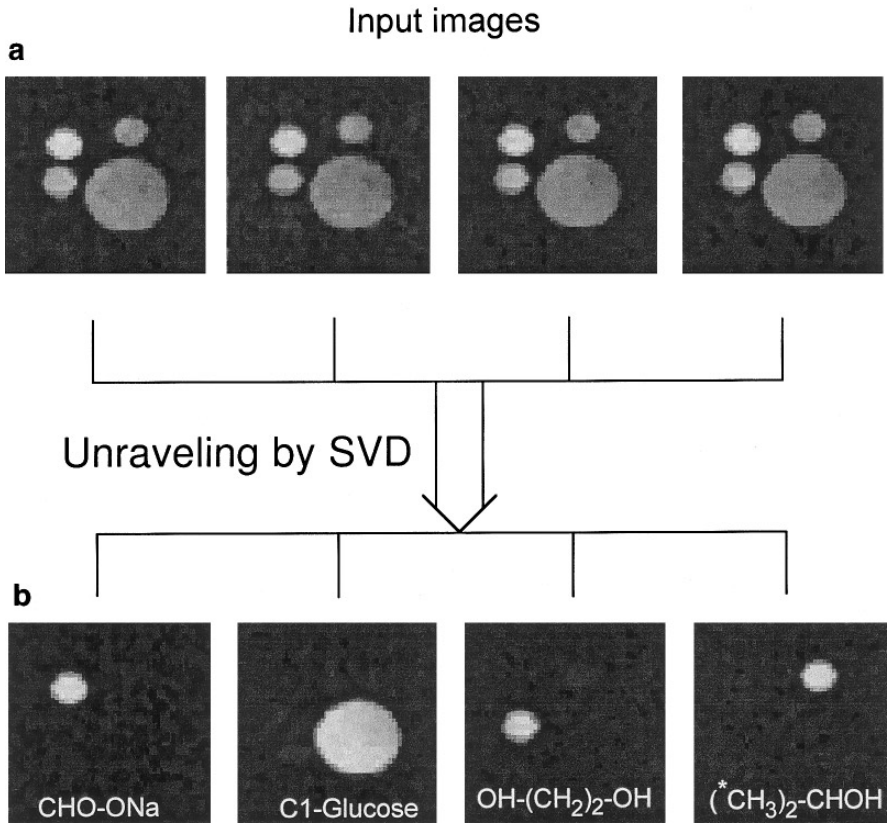

FIG. 4. Separation of ^{13}C spectroscopic images using MILS. (a) The input images obtained corresponding to the set of optimized time displacements δt_1: from left to right: $\{-116.16, -59.48, 55.27, \text{and } 111.96\ \mu s\}$, with τ and t_1 assuming values of 2.994 and 11.976 ms, respectively. (b) The resulting images segregated according to their respective line positions in the order of the spectrum as in Fig. 3 with the corresponding moieties identified as labeled. The third image from the left should consist of two components: ethylene glycol, the stronger component, observed as labeled, and a weaker component, the α-carbon of 2-propanol, too faint to make visible in the photograph.

in Fig. 5, of a series of experimental runs by using timing sets $\{\delta t_{1j}\}$ deliberately misset to correspond to increasingly larger κ. The resulting images were analyzed by evaluating a contamination index ρ and a noise index N defined, respectively, as

$$\rho \equiv \sum_{j}^{M} \frac{\langle G_j - \text{BGN}\rangle}{I_j}, \quad N \equiv \frac{\langle \text{BGN}\rangle}{\langle \text{Signal}\rangle}, \qquad [12]$$

where BGN stands for background noise and G_j and I_j are the ghost and genuine image intensities of the jth spectral lines, respectively (ghosts G_j are the mean image intensities that appear at compartments $i \neq j$). Note that when plotting N and ρ against κ, one finds that N increases nearly linearly while ρ does not change as the condition number is increased.

The second type is the same set of images in Fig. 4b but generated by the ^{1}H-based technique, an unappealing but only alternative if the conventional FT method must be used for inverse detection. As mentioned under Method and Materials, the ^{1}H-based CSI experiment can be performed in the same abridged manner if the supplementary spectrum is a ^{13}C-decoupled proton spectrum. In this case, the pulse sequence in Fig. 1 was run with a fixed t_1 while the timing of the proton refocusing pulse was then allowed to advance or delay from its original setting, TE/2, by a set of optimized time displacements $\{\delta t\}$ determined from the given spectrum. The results of this run are shown in Fig. 6. Even with the optimized settings and overdetermination ($N = 5$), the ''ghost'' images are clearly much more pronounced than the ^{13}C images shown in Fig. 4b.

The final issue needed to be considered for this technique is not unique to the scheme currently proposed but is pertinent to the more general HMQC techniques. What concerns us is the sensitive dependence of signal amplitude on the coupling constant J_{CH} according to Eqs. [3]–[5] for any given timing sets $\{\tau_j\}$ chosen for a particular J_{CH} according to the optimal condition as specified by Eq. [11]. As the coupling constants vary substantially among different moieties (e.g., in our phantom, the J_{CH} ranges from 126 Hz in the methyl carbon of 2-propanol to 192 Hz in the carboxyl carbon of sodium formate), it is futile to try to find timing

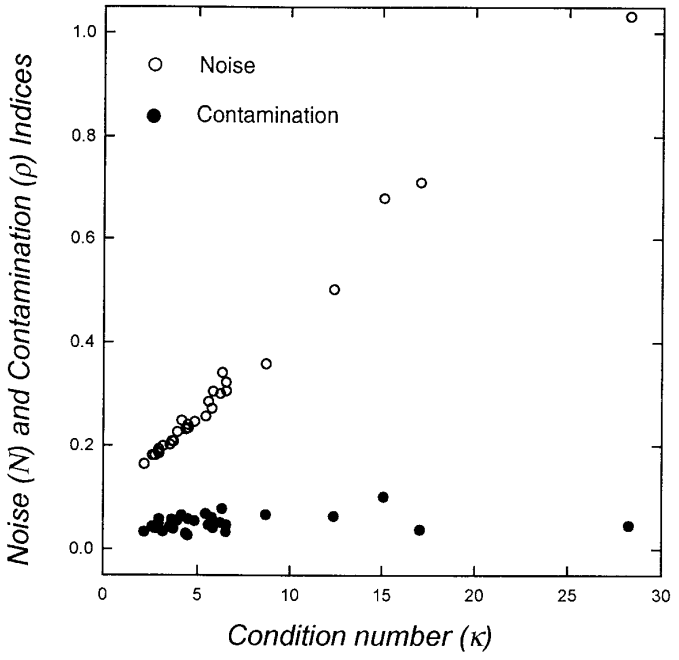

FIG. 5. Effect of nonideal time displacements on the separation of spectral images. Plots of contamination index ρ and noise-to-signal N as a function of the condition number κ. The definitions of ρ and N are given in Eq. [12].

sets $\{\tau_j\}$ that would be immune to such sensitivity. A more practical question is to ask how severe is this amplitude modulation in normal circumstances and how can it be alleviated. Intuitively, the best general strategy for minimizing its impact is to pick a set of $\{\tau_j\}$ as short as possible according to the optimized condition Eq. [11] (which means that $n = 1$) using a mean J_{CH} of the all carbon moieties. This conjecture was experimentally verified using the pulse sequence of Fig. 1 with a fixed t_1 and without the imaging gradients. Carbon-decoupled but ^{1}H-based spectra were acquired using a timing set $\{\tau_j\}$ optimized for each of four moieties in question (note that since our interest here is to determine how the signal amplitude of the CSI moieties is affected by the setting of $\{\tau_j\}$, the ^{1}H-based spectrum provides basically the same information and is therefore a legitimate shortcut substitute for its ^{13}C-based counterpart which is much more time consuming in its acquisition). Our results, not shown here because of their tediousness, indeed demonstrated that, for the integer $n = 1$ in Eq. [11], the timing sets $\{\tau_j\}$ chosen for ethylene glycol ($J_{CH} = 141$ Hz) and C1-glucose ($J_{CH} = 167$ Hz), which are close to the mean value 156.5 Hz, gave more uniform spectral intensity than the timing sets chosen according to the two extreme cases. In fact, the timing set used to generate the spectral images shown in Fig. 4 corresponds to the optimized condition based on the J_{CH} of glucose. For $n = 1$, the difference between the optimized and unoptimized lines, even in the worst cases, while not insignificant, is nevertheless far from overwhelming. For $n > 1$, however, the unoptimized lines deteriorate rapidly, rendering a strongly amplitude-modulated spectrum. Based on these observations, the sensible strategy of choosing the shortest $\{\tau_j\}$ set for a mean coupling constant among the moieties is reaffirmed.

DISCUSSION

The technique proposed seeks to garner the most important advantage of the inverse-detection scheme for ^{13}C via a proton, sensitivity enhancement, while preserving the strong attribute of ^{13}C, the large chemical shifts. In addition to these two most important features, there are other side benefits as well, one of which worth mentioning is the direct consequence of polarization transfer from ^{13}C to a proton. The benefit of converting a ^{13}C polarization to a proton one resides in the fact that the gradient amplitudes needed for many of the standard imaging applications, such as slice selection and phase and frequency encoding, are all scaled down by a ratio of γ_H/γ_C, or a factor of approximately 4 (*3*). There are other benefits as well, such as the relevant longitudinal relaxation is switching from the carbon to the proton spins which is beneficial since protons tend to have shorter T_1 values than ^{13}C. Based on this reasoning, the TR used in this set of experiments can be greatly shortened, thereby significantly cutting the total scan time even further. For a human study, however, this reduction may not be too

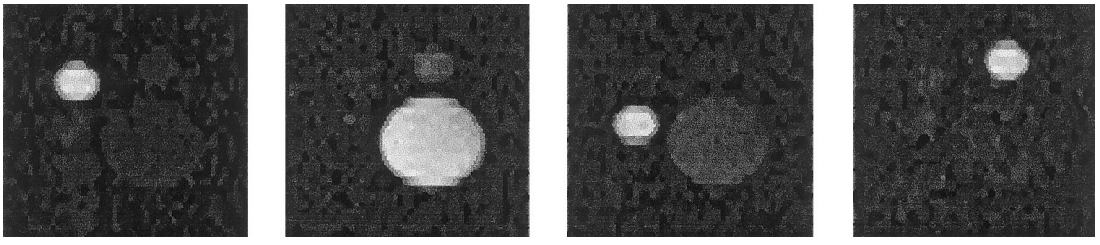

FIG. 6. ^{1}H-based ^{13}C component images obtained through the HMQC sequence. Images of different ^{13}C moieties separated based on the chemical shifts of the protons to which these moieties are coupled. Note that, in comparison with Fig. 4b, the ghost problem is significantly worse even when the images are acquired under optimized settings and with overdetermination ($N = 5$) ($\delta\tau$: $\{-566.83, -126.25, -56.53, 86.97, 731.22\ \mu s\}$).

substantial due to the safety concern of high RF duty cycle caused by the need of broadband decoupling. However, decoupling applied on the carbon spins is substantially safer than on protons since the frequency of the latter is four times higher.

It should be noted that exploitation of the large chemical shifts of ^{13}C using inverse detection has indeed been done previously in the form of 2D NMR (*11*) and even in chemical-shift imaging via frequency-selective excitation in the carbon channel (*9*). To compare the latter with the present scheme, the MILS scheme has the following distinct advantages in technical implementation over the frequency-selection technique: (1) The MILS scheme needs simple rectangular-shaped pulses while the frequency-selection technique requires an RF pulse with more restrictive bandpass such as the DANTE sequence. The implementation of such pulses makes it harder to satisfy the optimal timing conditions as specified in Eq. [11]. (2) Though a supplementary ^{13}C spectrum is helpful in determining the optimized condition for MILS (even this requirement is in practice unnecessary, as shown in Fig. 5, as far as spectral separation is concerned), the important spectral elements one needs to know are the approximate spectral spacing between the lines rather than their absolute positions. Consequently, the dependence of chemical-shift separation via MILS on the main-field homogeneity is relatively less critical than its frequency-selection counterpart. The frequency-selection technique also has an edge over the MILS scheme on two counts. First of all, as is often the case in biological applications, one is interested in only one or two of the ^{13}C moieties out of many lines in a spectrum; under such conditions, the frequency-selection technique is a better alternative since it is faster to selectively scan what is needed than trying to capture all components within the spectrum. Second, by scanning the spectral components one at a time, one can, in principle, tailor the time settings individually to avoid the amplitude modulation effect encountered in MILS. However, as mentioned earlier, the long duration requirement of the RF pulse in the frequency-selection technique greatly diminishes this advantage. Ultimately, the best compromise, in view of what has been said, is perhaps a combination of these two approaches—the application of MILS on a selected band of lines by the use of an RF pulse with a broader bandwidth just wide enough to cover the spectral range of interest. This will have the benefit of further reduction of scan time without the usual technical difficulty accompanying the frequency-selective pulse with narrow bandpass.

The feasibility of developing a ^{13}C HMQC-MILS technique into a useful *in vivo* application hinges upon the experimenter's capability of (i) successfully introducing key carbon moieties with adequate ^{13}C isotopic enrichment in the precursor for a particular physiologic process one wishes to follow; one important example is the use of ^{13}C-enriched glucose in a strategically chosen carbon position for the study of cerebral metabolism and brain function; and (ii) providing both proton and carbon RF fields with a sufficient degree of uniformity. This requirement is essential as the efficiency of polarization transfer between the two spin species depends on the tip angles of the RF pulses applied to them. The use of adiabatic pulses (*21*) with doubly tuned surface coils may solve the RF nonuniformity problem, but the long pulse-duration requirement in its implementation is in conflict with the short-time condition discussed earlier to avoid J_{CH}-induced amplitude modulation.

Besides these technical caveats, there are other difficulties inherently associated with the application of HMQC in biological tissues. First, as mentioned before, the benefit of sensitivity enhancement by polarization transfer can be realized only if the T_2 of the spin moieties is sufficiently long (T_2^* is presumably not a problem since the sequences for both spin species are spin echo in kind). When T_2 is short, signal enhancement deteriorates, and to make up for this loss, one needs to increase the number of accumulations n from the current value of 4 to 16 if such a loss amounts to halving the original signal. However, as the need for the increase of n heightens, the advantage of the method of polarization transfer over the conventional FT technique diminishes. Second, it is common in biological tissues that the carbon spectrum is dominated by a narrow band of peaks attributed to the phospholipids. These signals, while not as dominant in magnitude as water, are nevertheless an unwanted source of trouble causing dynamic range problems for the much weaker signals of the more interesting metabolites. There are many ways, besides the selective isotopic enrichment mentioned earlier, to alleviate this problem. The first is by frequency-selective saturation on the carbon signal. This can be accomplished by the application, prior to all the events shown in Fig. 1, of a frequency-selected 90° pulse at the center frequency of this fat multiplet with a bandwidth tailor matched to its width. The fat-selected transverse coherence following this pulse can then be dephased by homogeneity spoiling gradient pulses. By exploiting the fact that most of the animal fats are located anatomically in the subcutaneous layer of the skin surrounding the area of interest, an alternative scheme can be devised by avoiding the observation of the fat periphery via reduction of the FOV using spatial selection through the proton spin. For example, by replacing the hard 180° refocusing pulse on the proton in Fig. 1 by a slice-selection pulse, one-dimensional fat suppression can be achieved along the selected direction. Two-dimensional (or complete) avoidance can also be accomplished, if so desired, by delaying the observation of the proton signal to the second echo by the insertion of a second refocusing 180° pulse selected along an in-plane but orthogonal direction to the last pulse.

Finally, as demonstrated in our phantom experiments, the ^{13}C HMQC-MILS method requires, for best results, a proton-decoupled ^{13}C spectrum, *a priori,* of the tissue regions sub-

jected to the study. This requirement may pose a problem for any study at the beginning when the outcome of the end product is presumably unknown (unless the biochemical pathway of the process under study is well understood beforehand by other means). However, this problem should be moot as experiences and knowledge on the subject accumulate once the study passes through its initial phase of development.

REFERENCES

1. B. Künnecke, *in* ''C-13 NMR Spectroscopy of Biological Systems'' (N. Beckmann, Ed.), pp. 159, Academic Press, San Diego, (1995).
2. D. W. Kormos, H. N. Yeung, and R. C. Gauss, *J. Magn. Reson.* **71,** 159 (1987).
3. H. N. Yeung and S. D. Swanson, *J. Magn. Reson.* **83,** 183 (1989).
4. S. D. Swanson and H. N. Yeung, Abstracts of the Society of Magnetic Resonance in Medicine, 9th Annual Meeting, New York, p. 1067 (1990).
5. S. Yamai, H. Ikehira, T. Hashimoto, K. Mori, T. Maki, H. Fukuka, and Y. Ueshima, *Magn. Reson. Med.* **15,** 158 (1990).
6. R. E. Hurd and B. K. John, *J. Magn. Reson.* **91,** 648 (1991).
7. N. Beckmann and S. Müller, *J. Magn. Reson.* **93,** 186 (1991).
8. J. Ruiz-Cabello, G. W. Vuister, C. T. W. Moonen, P. van Gelderen, J. S. Cohen, and P. C. M. van Zijl, *J. Magn. Reson.* **100,** 282 (1992).
9. T. Inubushi, S. Morikawa, K. Kito, and T. Arai, *Biochem. Biophys. Res. Commun.* **191,** 866 (1993).
10. D. Freeman, N. Sailasuta, S. Sukumar, and R. E. Hurd, *J. Magn. Reson. B* **102,** 183 (1993).
11. P. C. M. van Zijl, A. S. Chesnick, D. DesPres, C. T. W. Moonen, J. Ruiz-Cabello, and P. van Gelderen, *Magn. Reson. Med.* **30,** 544 (1993).
12. A. Bax, R. H. Griffey, and B. L. Hawkins, *J. Magn. Reson.* **55,** 301 (1983).
13. W. T. Dixon, *Radiology* **153,** 189 (1984).
14. R. E. Sepponen, J. T. Sipponen, and J. I. Tanttu, *J. Comput. Assist. Tomogr.* **8,** 585 (1984).
15. Z. H. Cho, O. Nalcioglu, H. W. Park, J. B. Ra, and S. K. Hilal, *Med. Reson. Med.* **2,** 253 (1985).
16. A. Bax, A. F. Mehlkopf, and J. Smidt, *J. Magn. Reson.* **35,** 167 (1979).
17. X. Hu, D. N. Levin, P. C. Lauterbur, and T. Spraggins, *Magn. Reson. Med.* **8,** 314 (1988).
18. N. Li and H. N. Yeung, *IEEE Trans. Med. Imaging* **12,** 342 (1993).
19. C. L. Lawson and R. J. Hanson, ''Solving Least Squares Problems,'' Prentice–Hall, Englewood Cliffs, NJ (1974).
20. N. Li, Ph.D. dissertation, University of Michigan, Ann Arbor, MI (1993).
21. D. G. Schupp, H. Mekle, J. M. Ellermann, Y. Ke, and M. Garwood, *Magn. Reson. Imaging* **30,** 18 (1993).